5-31-2023

Engineering a multicompartment in vitro model for dorsal root ganglia phenotypic assessment

Sydney M. Caparaso

Adan Redwine

Rebecca A. Wachs

Received: 23 December 2022 | Revised: 19 May 2023 | Accepted: 31 May 2023

DOI: 10.1002/jbm.b.35294

RESEARCH ARTICLE

Engineering a multicompartment in vitro model for dorsal root ganglia phenotypic assessment

Sydney M. Caparaso | Adan L. Redwine | Rebecca A. Wachs

Department of Biological Systems Engineering, University of Nebraska-Lincoln, Lincoln, Nebraska, USA

Correspondence
Rebecca A. Wachs, Department of Biological Systems Engineering, University of Nebraska-Lincoln, Lincoln, NE, USA.
Email: rebecca.wachs@unl.edu

Funding information
NSF Career Award Grant, Grant/Award Number: 1846857; NIH/NIGMS Grant, Grant/Award Number: T32 GM136593; NSF Award, Grant/Award Number: 2152065

Abstract

Despite the significant global prevalence of chronic pain, current methods to identify pain therapeutics often fail translation to the clinic. Phenotypic screening platforms rely on modeling and assessing key pathologies relevant to chronic pain, improving predictive capability. Patients with chronic pain often present with sensitization of primary sensory neurons (that extend from dorsal root ganglia [DRG]). During neuronal sensitization, painful nociceptors display lowered stimulation thresholds. To model neuronal excitability, it is necessary to maintain three key anatomical features of DRGs to have a physiologically relevant platform: (1) isolation between DRG cell bodies and neurons, (2) 3D platform to preserve cell–cell and cell-matrix interactions, and (3) presence of native non-neuronal support cells, including Schwann cells and satellite glial cells. Currently, no culture platforms maintain the three anatomical features of DRGs. Herein, we demonstrate an engineered 3D multicompartment device that isolates DRG cell bodies and neurites and maintains native support cells. We observed neurite growth into isolated compartments from the DRG using two formulations of collagen, hyaluronic acid, and laminin-based hydrogels. Further, we characterized the rheological, gelation and diffusivity properties of the two hydrogel formulations and found the mechanical properties mimic native neuronal tissue. Importantly, we successfully limited fluidic diffusion between the DRG and neurite compartment for up to 72 h, suggesting physiological relevance. Lastly, we developed a platform with the capability of phenotypic assessment of neuronal excitability using calcium imaging. Ultimately, our culture platform can screen neuronal excitability, providing a more translational and predictive system to identify novel pain therapeutics to treat chronic pain.

KEYWORDS
dorsal root ganglia, in vitro device, neuronal excitability, peripheral sensitization, phenotyping

1 | INTRODUCTION

Chronic pain is the leading source of disability and disease in the world and affects up to 20% of people during their lifetime in the United States.[1–3] Current treatments for chronic pain commonly include pharmacological therapeutics and surgical intervention; however, chronic pain treatments are limited and have high rates of adverse effects.[4,5] Some common methods for identifying therapeutics to treat chronic pain include probing molecular pathways and assessing pain-like behavior in animal models.[6–11] While these

methods have provided foundational knowledge about the molecular pathways that drive many pain states, the lack of clinical translation of pain treatments from these findings highlights an unmet need for screening models with better predictive capability.

Phenotypic screening platforms rely on modeling and assessing high-level pathologic function, rather than molecular changes and are therefore more likely to impact painful pathology. Thus, phenotypic screening platforms can have a stronger predictive capability.[6,9,12] For example, chronic pain patients present with pathology such as lowered pain thresholds.[13–15] These lowered pain thresholds can be caused by noxious inflammatory or mechanical stimuli in peripheral tissue that repetitively stimulates nerves.[15–18] Repeated stimulation of peripheral nerves due to noxious inflammatory and mechanical factors can result in an increased neuronal excitability, which presents pathologically as a lowered pain threshold.[14,15,19–21] Traditional molecular screening relies on targeting specific ion channels and signaling cascades that eventually lead to lowered pain thresholds, but these molecular changes do not always scale back up to alleviate painful pathology. However, phenotypic screening relies on higher order changes in neuronal behavior (such as firing threshold) which correlate more directly to the painful pathology.[6] Since phenotypic screening platforms have closer proximity to the painful pathology and do not require knowledge of molecular targets, they have an increased potential for translational efficacy. Importantly, a review by Swinney et al.[22] showed that the majority of first-in-class small molecule drug therapeutics approved by the food and drug administration from 1999 to 2008 were identified from phenotypic screening compared to target-based screening. This review suggests that the identification of molecules with appropriate (and potentially multiple) targets may not emerge as quickly or at all from following a focused target-based approach since the nuanced interaction between drug and target may be missed.

A phenotypic screening platform that models heightened neuronal excitability present in chronic pain patients is a promising tool for

TABLE 1 Literature review of current DRG culture platforms indicating if each platform meets the three physiological criteria of DRG culture, as outlined.

Culture platform		Isolation	Native support cells	Environment			References
				3D	Substrate	Substrate coating	
Petri dish		−		−			
3D Hydrogel	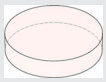	−	+	+			
Campenot		+	−	−	Polystyrene	Collagen	Jonas et al.[23] Ponce et al.[24] Klusch et al.[25] Campenot et al.[26]
Explant chamber		+	+	−	Polystyrene	Poly-D-lysine and laminin	Vogelaar et al.[27]
Boyden chamber		+	+	−	Glass	Poly-D-lysine and laminin	Ying et al.[28]
Neuron-oligodendrocyte co-culture device	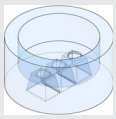	+	−	−	Glass	Matrigel on poly-D-lysine	Ristola et al.[29]
Multi-nodal neural network microfluidic chip	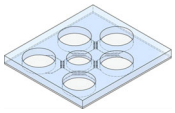	+	−	+	Glass	Poly-L-ornithine and laminin	Wijdeven et al.[30]
Dipartite microfluidic system	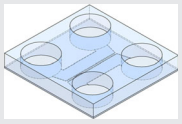	+	−	−	Glass (or) Polystyrene	Poly-L-lysine Poly-D-lysine Poly-L-ornithine	Silva et al.[31] Jia et al.[32] Park et al.[33] Sundaramoorthy et al.[34]
			+	−	Glass	Poly-D-lysine	Leitao et al.[35]
Tripartite microfluidic system	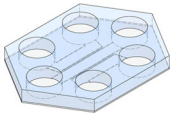	+	−	−	Glass (or) Lumox	PLL PDL and laminin 1	Vysokov et al.[36] Jocher et al.[37] Dumoulin et al.[38]

Abbreviation: DRG, dorsal root ganglia.

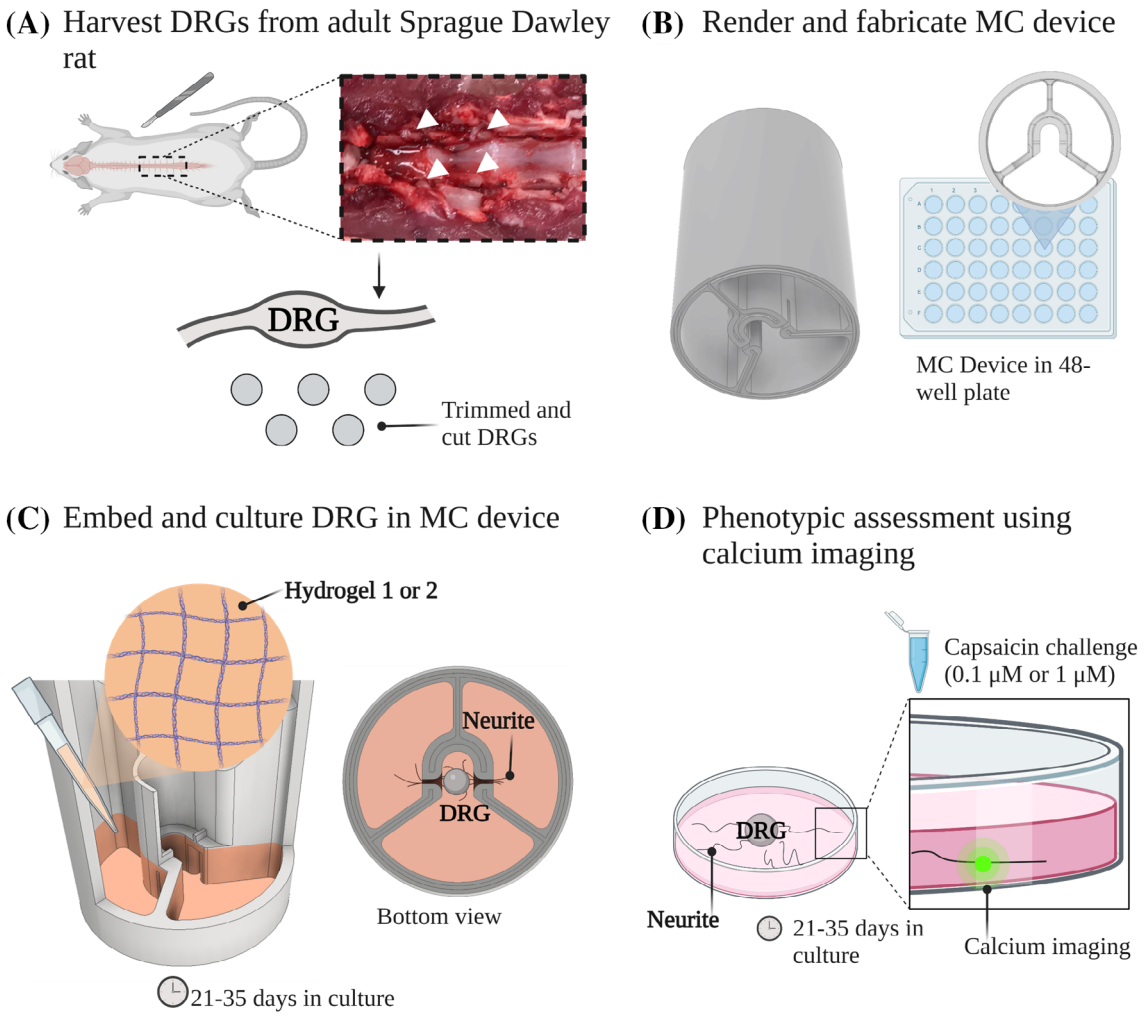

FIGURE 1 Schematic depicting experimental processes. (A) Dorsal root ganglia (DRG) harvest from adult Sprague Dawley rats. (B) Render and fabricate multicompartment (MC) device. (Right) MC device secured in 48-well plate. (C) DRG explant embedding and culture within the collagen-laminin-methacrylic anhydride hyaluronic acid hydrogels. (D) DRG phenotypic assessment with fluorescent calcium imaging to assess neuronal excitability. Schematic made in Biorender.

discovery of novel drugs to treat this pain. Review of the literature highlights three key anatomical criteria that are necessary to mimic in vitro to maintain relevance to the in vivo environment, (1) maintaining isolation between distal neurites and DRG cell body, (2) presence of three-dimensional environment, and (3) presence of native non-neuronal support cells. However, a literature review of current dorsal root ganglia (DRG) culture models yields no culture systems that incorporate these three features——to our knowledge——, highlighting a gap in the field (Table 1).[23–38] Thus, the goal of this work was to develop a physiologically relevant phenotypic screening DRG platform of neuronal excitability that maintains key anatomical features to recapitulate the in vivo environment (Figure 1).

1.1 | Maintain isolation between distal neurites and DRG cell body

DRGs are located adjacent to the spinal cord and contain a cluster of primary sensory neuron cell bodies whose neurites extend into peripheral tissue, anatomically and environmentally isolated from the cell bodies.[20,39,40] Noxious stimuli at the peripheral site of inflamed or diseased tissues initiates pain by acting directly on pain-sensing neurites (nociceptors), distant from the DRG cell bodies.[20,41–43] In vitro, this isolation can be modeled using compartmentalized devices which separate DRG cell bodies and neurites with a barrier that allows neurite growth between compartments while limiting fluidic diffusion.[44] A commonly used platform to model DRG isolation is the Campenot chamber[45] which uses a Teflon divider to create two or three compartments to mimic the in vivo isolation (Table 1).[45–47] However, the Campenot chamber can only be used with dissociated DRG neurons in 2D, which disrupts the native cellular composition and decreases physiological relevance, specifically neuronal excitability.[48,49] Dissociation is the process in which DRG cells are disrupted by mechanical agitation to produce primary neurons; however, it is also common to remove non-native support cells in this process due to over proliferation.[50–52] In this study, we developed a compartmentalized device for culture of explant DRGs with spatial fluidic isolation between DRGs and neurons.

1.2 | Three-dimensional environment

There is growing consensus that 3D culture conditions are more relevant because cell–cell and cell-extracellular matrix interactions are more like those present in vivo.[48,53–58] Specifically, previous work has shown that the stiffness of the culture environment influences axonal growth,[59,60] branching,[61] and neuronal excitability of DRGs.[45,57] Despite this knowledge, the majority of in vitro DRG platforms utilize 2D culture, as represented in Table 1.[23–25,45] Commonly, the methods of 2D DRG culture include direct plating onto a rigid surface or onto a coating of varying substrate stiffness.[39,62–66] However, in 3D culture, cells are embedded within a matrix where the mechanical properties are tunable by modifying the composition.[61,67–70] Specifically, increasing matrix stiffness of a 3D hydrogel has been correlated with decreased neurite length of sensory neurons from neonatal rat superior cervical ganglia[71]; therefore, it is important to use a matrix with mechanical properties that mimic native neuronal tissue. It is important to note that both dissociated and 3D explant DRGs have been cultured in 3D matrices in previous literature, as indicated in Table 1. In our study, we used collagen type I, methacrylated hyaluronic acid (MAHA), and laminin hydrogels to promote cell–cell and cell–extracellular matrix interactions and to maintain physiologically relevant mechanical and diffusivity properties that mimic native tissue.

1.3 | Presence of native non-neuronal support cells

In vivo, the presence of non-neuronal support cells such as Schwann cells and satellite glial cells (SGC) are important for function of peripheral sensory neurons in both healthy and hyperexcited states.[39,62–66] Schwann cells encapsulate axons, forming the myelin sheath that allows for saltatory signal transduction.[64] In addition, SGC are essential glial cells in sensory ganglia and are critical for DRG function. SGCs envelop the cell bodies of DRGs and have a role in sensory signaling.[65] In chronic pain conditions, activation of Schwann cells and SGCs has been correlated with increased levels of pro-inflammatory cytokine secretion, which is implicated in increased nociceptor excitability.[66] To date, most studies using compartmentalized culture platforms to characterize DRG phenotype have used dissociated DRGs (Table 1). However, the use of DRG explants to maintain non-neuronal support cells is established in the field and results in more relevant neuronal excitability; therefore, it is an advantageous method for phenotypic screening.[46,72–74] Specifically, explant DRGs that maintained non-neuronal support cells have been used in multicompartment (MC) devices (Table 1). In this study, we used adult rat DRG explants in a compartmentalized device to ensure the presence of non-neuronal support cells.

Despite many studies using compartmentalized culture platforms, to our knowledge there are no current culture platforms that maintain all three key anatomical features of the in vivo environment (Table 1). We have engineered a 3D MC culture platform that (1) maintains isolation between distal neurites and DRG cell bodies, (2) uses a three-dimensional hydrogel of relevant stiffness, and (3) includes native non-neuronal support cells that can be used as a phenotypic screening platform to measure neuronal excitability by using calcium imaging.

2 | MATERIALS AND METHODS

2.1 | Hydrogel fabrication

Throughout this study two unique hydrogel formulations were used due to differences in diffusivity properties. The two fabrication processes and two formulations are described in detail below. Herein, the hydrogel formylations will be referred to as hydrogel 1 and hydrogel 2.

Hydrogel 1 contains the following components: methacrylated hyaluronic acid (MAHA, 53747-10G, Sigma-Aldrich) at 1.25 mg/mL, collagen type I rat tail at (50,205, Ibidi) at 4.5 mg/mL, laminin (3446-005-01, R&D Systems) at 0.75 mg/mL, 0.15% Irgacure (2-Hydroxy-4′-[2-hydroxyethoxy]-2-methylpropiophenone, 410896-10G, Sigma-Aldrich), 1× Dulbecco's Modified Eagle's Medium (DMEM, D2429-100ML, Sigma-Aldrich), and sodium bicarbonate (S6014-500G, Sigma-Aldrich) at 23.125 mg/mL. To fabricate *hydrogel 1*, hyaluronic acid (HA) was methacrylated with methacrylic anhydride (276685, MilliporeSigma) groups following previously established methods.[75–77] Hydrogels prepared for this study used MAHA with a methacrylation range of 85.0%–115.0%, which has been demonstrated in previous literature to promote neurite outgrowth and maintain robust mechanical properties.[76,78] The degree of methacrylation of MAHA was validated using nuclear magnetic resonance to detect hyaluronic acid and water peaks (data not shown) using methods previously described.[76] To prepare MAHA, 0.6% Irgacure was dissolved in a solution of 80% vol/vol concentrated DMEM/HEPES solution and 20% vol/vol 1× PBS. Then, 5 mg/mL MAHA was dissolved in Irgacure-DMEM solution for 48–72 h at room temperature in the dark with gentle agitation. On the day of gel fabrication, type I collagen was neutralized immediately prior to experimentation. For neutralization, 2% 1 M sodium hydroxide (NaOH, 221465-500G, Sigma-Aldrich), 4% milliQ H_2O, and 84% type I collagen at 8 mg/mL was combined and then buffered with 10% 10× PBS and the solution was mixed vigorously on ice with a pipette and the pH was tested using litmus paper. Neutralized type I collagen solutions with a pH between 6.8 and 7.8 were used. For the final hydrogel concentrations, neutralized type I collagen (2.5 mg/mL) was then rigorously mixed with MAHA (2.5 mg/mL), laminin (0.75 mg/mL), and 1× phosphate buffered saline (PBS) to create *Hydrogel 1*. *Hydrogel 1* was thermally crosslinked for 30 min at 37°C in an incubator then UV-crosslinked for 90 s with a high intensity UV lamp (UVP B 100-AP, Analytik) with a power of 12.5 ± 2.5 W/cm^2. *Hydrogel 1* was used for diffusivity, gelation, rheology, neurite growth, immunohistochemistry, and calcium imaging experiments in this study.

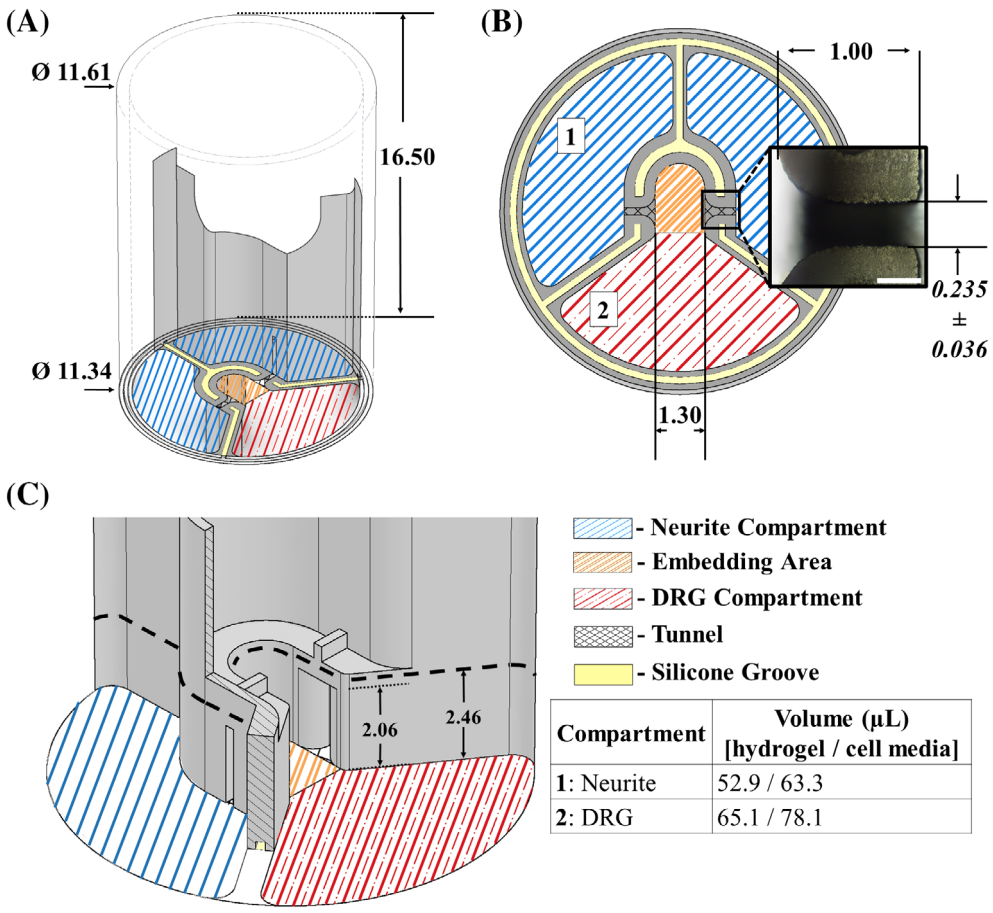

Compartment	Volume (µL) [hydrogel / cell media]
1: Neurite	52.9 / 63.3
2: DRG	65.1 / 78.1

FIGURE 2 Computer aided design of multicompartment (MC) device showing distinct compartments and features. (A) Angled side view of MC device displaying height and outer diameters. Outside of MC device has been made transparent to allow for visualization of interior. (B) Bottom view of MC device displaying dimensions of tunnels and embedding area. Magnified view displays image of tunnel in fabricated device. (C) Cut side view of MC device core depicting height of tunnel and hydrogel. Outside of the MC device has been made transparent for visualization of interior. Volumes for hydrogel and media per compartment displayed in table. Scale bar = 0.250 mm. All dimensions displayed in mm. Italicized measurement from fabricated device. Non-italicized dimensions correspond to computer aided design model. DRG, dorsal root ganglia.

Hydrogel 2 follows the same fabrication process as *hydrogel 1* outlined above. However, *hydrogel 2* has a final composition of 2.5 mg/mL MAHA, 2.5 mg/mL type I collagen, and 0.75 mg/mL laminin. *Hydrogel 2* was thermally crosslinked for 30 min at 37°C in an incubator then UV-crosslinked for 110 s with a high intensity UV lamp (UVP B 100-AP, Analytik) with a power of 12.5 ± 2.5 W/cm^2. *Hydrogel 2* was subjected to a longer UV-crosslinking period to account for the additional MAHA.[79] *Hydrogel 2* was used for diffusion, gelation, rheology, and neurite growth experiments in this study.

2.2 | Maintaining isolation between distal neurites and DRG cell bodies

2.2.1 | Device design and fabrication

A MC device with three distinct compartments was designed and fabricated to maintain fluidic isolation between DRG cell bodies and neurites in culture for up to 72 h. The MC computer-aided design (CAD) model was rendered using AutoDesk Inventor 2022. The MC CAD model was exported as a STL file and uploaded to a Form 3 (Formlabs) SLA 3D printer using Preform 3.23.1 software (Formlabs). The printer was calibrated according to manufacturer's standards and devices were printed using High Temp V2 (FLHTAM02, FormLabs) resin with a layer height of 25 µm. The highest aspect ratio (length-to-width) of the tunnels was determined by assessing the resolution of the 3D printer to print tunnels of varying lengths and widths. Tunnel lengths of 1.2, 1.0, 0.8, and 0.6 mm were printed with widths of 0.250, 0.225, 0.200, 0.175, 0.150, 0.125, and 0.100 mm. The successful formation of tunnels was assessed visually using a surgical microscope (WL37166, Carl Zeiss Microscopy, Inc.).

3D printer testing showed intermittent ability to print tunnels at 0.200 mm in width (data not shown); however, consistent successful tunnel formation was achieved at widths ≥0.225 mm, and therefore this dimension was used as the tunnel width in this device. Tunnel geometry was chosen to minimize the cross-sectional area and maximize length of the tunnel, thereby minimizing diffusion between compartments while still allowing robust neurite growth into the outer compartments. The final devices had a tunnel length of 1.0 mm and width of 0.250 mm (Figure 2B). A single connecting tunnel between compartments was used instead of multiple due resolution limitations of the 3D printer. Two outer neurite compartments were selected to allow treatment and control compartments during experimentation.

After printing, the final devices were washed using a Form Wash (Formlabs) for 60 min in isopropanol (>96%). Once washed, devices were post-cured at 80°C for 120 min in a Form Cure (Formlabs) at 405 nm. The devices were then thermally cured in an oven at 160°C for 180 min and sterilized via autoclave for 45 min on gravity cycle.

2.2.2 | Validation of maintaining isolation between compartments in MC device

To evaluate the diffusivity of *hydrogels 1* and *2*, a diffusion assessment was performed in a 6.5 mm hanging transwell system with a 0.4 μm polymer membrane (230635, Celltreat). One hundred micro liters of *hydrogel 1* and *2* was added to respective transwell inserts and crosslinked according to the methods described above in Section 2.1. After gelation, 100 μL of varying molecular size fluorescein isothiocyanate (FITC)-dextran solutions at 0.25 mg/mL in 1× PBS were added on top of the hydrogel into the transwell insert. FITC solutions of size 10 kDa (FD10s-100MG, Sigma-Aldrich) or 150 kDa (46946-100MG-F, Sigma-Aldrich) were used in this study. The inserts were then loaded into a well of a 24-well plate with 800 μL of 1× PBS to maintain the same fluidic height between the buffer solution and FITC-dextran to remove pressure differentials and ensure diffusion is concentration-driven. The amount of FITC that diffused through the hydrogel was determined by removing 30 μL of volume from the buffer solution, transferring the volume to a 96-well plate, and measuring the fluorescence at 485 ± 45 nm excitation and 525 ± 45 nm emission using a plate reader (Synergy, Biotek). Media aliquots were immediately added back to the transwell inserts after measurement. Fluorescent measurements were collected at time 0, 24, 48, and 72 h. Diffusion across the hydrogel was assessed for up to 72 h, which is the longest period most cells are left in culture between media changes. FITC solutions (10 and 150 kDa) at 0.25 mg/mL in 1× PBS were measured in parallel with sample time points and the resulting fluorescence was considered 100% fluorescence for the respective FITC sizes and deemed "FITC control." For each measurement of the sample aliquot, the fluorescence was calculated as a relative percentage of the FITC control. A total of $n = 3$ experiments were performed with triplicate hydrogels of each type (*hydrogel 1* and *hydrogel 2*) for each experiment.

To assess diffusion across compartments, devices were secured to a well in 48-well plate by applying sterile vacuum grease (077472132287, DOWCOR) to the bottom of the devices within the silicone grooves (Figure 2B) and allowed to dry overnight, and then of 52.9 μL *hydrogel 1* or *2* was added to each neurite compartment and 65.1 μL of *hydrogel 1* or *2* was added to the DRG compartment. *Hydrogels 1* and *2* were thermally crosslinked according to the methods outlined above in Section 2.1. 63.3 μL of FITC-dextran solutions at 0.25 mg/mL in 1× PBS with either 10 or 150 kDa were added on top of the left neurite compartment. 63.3 μL of 1× PBS was added to the remaining in the adjacent neurite compartment and 78.1 μL of 1× PBS was added in the DRG compartment to maintain the same fluid height between all compartments. The amount of FITC that diffused through the hydrogel was determined by removing 30 μL of volume from the buffer solution from each compartment, transferring the volume to a 96-well plate, and measuring the fluorescence at 485 ± 45 nm excitation and 525 ± 45 nm as outlined above in Section 2.2.2. Following each measurement, the aliquots were added back to the respective compartments to maintain matched compartment fluidic heights. The fluorescence from each compartment was compared to FITC control solutions, as outlined above in Section 2.2.2, to determine diffusion between compartments. A total of $n = 3$ experiments were performed with triplicate hydrogels for each type (*hydrogels 1* and *2*) for each experiment.

2.3 | Three-dimensional environment

2.3.1 | DRG explant isolation

All animal experiments were performed in accordance with the Guide for the Care and use of Laboratory Animals and approved through the University of Nebraska-Lincoln's Institutional Animal Care and Use Committee. Female Sprague Dawley rats aged 14–24 weeks were purchased from Charles River and humanely euthanized with CO_2 inhalation followed a bilateral pneumothorax. Blood was subsequently drained through the ventral side of the animal. Following euthanasia, rats were placed ventral side down on a sterile pad and sprayed with 70% EtOH. The skin was removed using blunt-nosed scissors along the length of the spine to visualize the musculature. Muscle was then removed around the spine using sharp-nosed scissors to expose the vertebra. Straight cup Rongeurs (16004-16, Fine Science Tools) were used to remove spinous and transverse processes T8-L6. When removing the articular processes, the Rongeur was kept parallel to spine to maintain consistent removal depth of about halfway down each facet. The spinal cord was gently lifted with forceps and removed using small sharp-nosed scissors (14094-11, Fine Science Tools) to carefully cut through bilateral attached nerve roots that remained connected to DRGs. Bilateral DRGs were visualized and removed using forceps and small straight edge spring scissors (15024-10, Fine Science Tools) by sterile dissection and immediately placed in cold sterile complete DRG media consisting of 86% Neurobasal A basal media (1088022, Fisher) supplemented with 4% fetal bovine serum (FBS, 26140079, Gibco), 1% penicillin/streptomycin (15140122, Fisher), 1% GlutaMax (35050061, Fisher), and 1% Vitamin B27 (17504044, Gibco). Excess tissue and nerve roots surrounding the DRG cell bodies were trimmed, and the cell body was cut into pieces ~0.3 mm in diameter. DRGs were embedded in three-dimensional (3D) hydrogels as previously described.[76] In short, one DRG piece was centrally embedded into the hydrogel and the hydrogel was crosslinked as described above in Section 2.1.

2.3.2 | Validation of DRG growth in three-dimensional MC environment

After preparing the hydrogels and securing the device into the 48-well plate, 52.9 μL volume of *hydrogel 1* or *2* was added to each neurite compartment and 65.1 μL of *hydrogel 1* or *2* was added to the DRG compartment to maintain a uniform gel height throughout the well. Trimmed DRGs were carefully placed centrally in the *x*–*y* plane of the embedding area and halfway down the hydrogel in the *z*-plane (Figure 2). Location in the *x*–*y* plane is confirmed with a widefield

microscope before gelation and the position can be adjusted if needed. Protrusions are included on the device indicating the position of the tunnels from above (Figure 2C). After embedding, hydrogels were crosslinked according to the methods outlined above in Section 2.1. DRGs in MC devices were cultured in complete DRG media as outlined above in *DRG explant isolation*. 63.1 µL of media was added to each neurite compartment and 78.1 µL media was added to the DRG compartment. Half media changes were completed every 3 days. For quantifying neurite length, control DRGs were embedded in 250 µL *hydrogel 1* or *2* only, without MC devices, and cultured according to the methods in *DRG explant isolation*. After 28 days, DRGs with and without MC devices in *hydrogels 1* and *2* were fixed for 1 h with 4% paraformaldehyde (PFA, 441244, Sigma-Aldrich), washed 3 × 15 min with 1× PBS and stored at 4°C. Brightfield images at 4× magnification were collected using a cell imaging plate reader (Cytation 1, BioTek) over a range of focal distances to collect data for all neurites. After acquiring a z-stack, the images were combined into a 2D rendering with in-focus features of all neurites. This allowed a representative assessment of whole DRG morphology while protecting the data from each unique image. Images were brightness and contrast enhanced for ease of neurite visualization. The objective of the system is to promote robust neurite outgrowth into the outer compartment to allow experimentation of isolated neurites. Due to constraints of the MC device design, not all neurites will grow into the outer compartments; however, this is not necessary for adequate function. Since the longest 3–5 neurites are generally observed to grow through the tunnels into the outer compartments of the MC device, the same number of neurites from plain control hydrogels were quantified. Therefore, the neurite length of the 3–5 longest neurites per DRG was manually selected and measured by one blinded observer from the maximum projections of Z-stacks using SimpleNeuriteTracer (Fiji, ImageJ) an accurate tool for semi-automated neurite length tracing.[49,76,78] A total of $n = 3$ independent experiments with unique culture were performed with 3–5 DRGs for each experiment. Neurites (3–5) per DRG were averaged to account for 13–15 DRGs per condition.

2.3.3 | Characterization of three-dimensional environment

Gelation kinetics assesses the amount of light absorbed by the gel over time at 405 nm. This process indicates fibril formation as the gel becomes increasingly opaque as collagen fibrillation occurs, which suggests collagen crosslinking.[76,78] One hundred micro liters of *hydrogel 1* and *2* was pipetted in triplicate into a 96-well plate and placed into a 37°C preheated microplate reader and the absorbance was read every minute for 30 min. The change in absorbance was calculated as the normalized absorbance from $NA = \frac{A2-A1}{Max-A1}$ where NA is the normalized absorbance, *A2* is absorbance at a specific time point, *A1* is the initial absorbance, and Max is the maximum absorbance over the data series.[78]

Rheological characterization of *hydrogel 1* and *2* was performed and compared to previously published data on various neuronal tissue to verify the hydrogels were within the same range of moduli as native neuronal tissue.[80,81] Mechanical properties were assessed using an Anton Paar MCR 203 with sand-blasted plates to reduce slippage and a humidity bath using methods as described in Piening et al.[78] Briefly, hydrogels were mixed as described above in Section 2.1, and then the solution was injected into 8-mm diameter silicone molds (666305, Grace Bio-Labs) and secured between two glass slides using a 21-gauge needles (305129, BD). The molds were thermally gelled at 37°C for 30 min, followed by UV crosslinking for 90 or 110 s for *hydrogel 1* and *hydrogel 2*, respectively. The gels were then removed from the molds and soaked in 1× PBS for 30–60 min. Initially, an amplitude sweep was performed to determine the strain value within the linear viscoelastic region of the hydrogels. The linear viscoelastic region was determined to be 0.01% strain and a frequency sweep was performed at this strain rate from 0.1 to 100 rad/s with 20 data points collected. Each run was performed with the temperature set to 37°C in a humidity bath. Prior to each run, the gel was subjected to a 1-min equilibration period on the rheometer stage.[78] Data were calculated for the storage (G') and loss (G'') modulus. The dynamic shear modulus (G^*) was calculated as $G^* = \sqrt{G'^2 + G''^2}$ and tan δ was calculated as $\tan\delta = G''/G'$. A total of $n = 3$ experiments were performed with triplicate hydrogels for each experiment.

2.4 | Presence of native non-neuronal support cells

2.4.1 | Validation of native non-neuronal support cells

Immunostaining on DRG explants cultured in *hydrogel 1* (4.5 mg/mL type 1 collagen, 1.25 mg/mL MAHA, 0.75 mg/mL laminin) was performed to validate presence of native non-neuronal support cells. DRGs were fixed in 300 µL of 4% PFA (441244-1KG, Sigma-Aldrich) for 1 h at room temperature at day 14 in culture after robust neurite growth was observed. DRGs were then washed with 1× PBS for 3 × 15 min and stored in 1× PBS at 4°C until immunostaining. Fixed DRGs in gels were stained for Schwann cells (SOX10),[82] SGCs (CD11b), and microtubules (β-III-tubulin). The cells were permeabilized in 200 µL of blocking buffer (0.5% Triton X-100 [93443, Sigma-Aldrich] and 4% goat serum [G9023, Sigma-Aldrich] in 1× PBS) for 1 h at room temperature with gentle agitation of 100 rpm. The blocking buffer was removed and 200 µL of primary antibodies against SOX10 (Ab155279 Abcam, 1:1000), CD11b (MCA275R, Bio-Rad. 1:500), and β-III-tubulin (NB100-1612, Novus Biologicals, 1:500) were added to each well for 36 h at 4°C. The primary antibody was removed from each well, and the gels were washed 3 × 4 h in PBST (0.05% Tween 20 [BP337, Fisher Scientific] in 1× PBS) with gentle agitation at room temperature. Secondary antibodies for SOX10 (α-rabbit 488, ab150081, Abcam, 1:500 in blocking buffer), CD11b (α-mouse 555, ab150118, Abcam, 1:500 in blocking buffer), and β-III-tubulin (α-chicken 647, a21449, Thermo Fisher, 1:500 in blocking buffer) were added and incubated overnight at 4°C protected from light. The secondary antibodies were removed, and the gels were

washed 3 × 4 h in PBST at room temperature, with gentle agitation, protected from light and stored in 1× PBS at 4°C until imaged. Following staining, the gels were removed from the well plate and transferred to a petri dish for imaging using Confocal microscope (LSM 800, Carl Zeiss Microscopy, Inc.) at 488, 555, and 647 nm with 10 and 20× objectives. Triplicate DRGs from two rats were imaged.

2.4.2 | Assessment of neurite phenotype

Calcium indicator dyes are a common method to measure neuronal excitability since intracellular calcium dynamics during depolarization closely model the firing frequency of action potentials which can serve as an indirect measure of neuronal excitability.[41,83] Upon binding of calcium ions, indicator dyes undergo a conformational change resulting in an emission of a photon which can be measured with fluorescent imaging.[84] Herein, calcium imaging was used to investigate the functional properties of neuronal excitability by agonizing DRGs with capsaicin, which activates TRPV1+ neurites through binding the ion channel's transmembrane segments.[83] Explant adult rat DRGs were harvested and embedded in 250 µL of *hydrogel 1* in a 48-well plate, as described above in Sections 2.3.1 and 2.1, respectively. A sterile 2 nM stock solution of Oregon Green BAPTA-488 (O6807, Fisher) was prepared in dimethyl siloxane (DMSO) and sonicated for 5 min at ambient temperature. A working solution of 2 µM Oregon Green BAPTA-488 was prepared with 0.04% Pluronic F-127 (P3000MP, Sigma) and DRG media as described above. One hundred and fifty microliters of 2 µM Oregon BAPTA-488 in complete DRG media was added to attain a final in-well concentration of 1 µM. The DRGs were incubated at 37°C with the fluorescent probe for 1 h. After incubation, the DRGs were washed 3 × 5 min by removing 200 µL of the well contents and replacing with fresh complete DRG media for each wash, to remove unbound probe. The intact gels with embedded DRGs were transferred from a 48-well plate to a petri dish and immediately imaged with a confocal microscope (LSM 5 Exciter, Carl Zeiss Microscopy, Inc.) with a 10× objective and a 488 nm laser. A scan area containing at least three unique neurites at a consistent *z*-depth was selected for imaging, and the scan area was adjusted to contain the distal terminal of each neurite within the frame. The hydrogel was spiked with 100 nM capsaicin and 1 µM capsaicin (75 µL in 1× PBS) (as seen in Figure 7A) and the neurites were imaged using high-speed confocal microscopy with a frame rate of 1 Hz and size of 512 × 512. The hydrogels were washed for 2 × 5 min with complete DRG media between the two capsaicin challenges. DRGs were recorded for 2 min for each trial.

The fluorescence was analyzed by the average of all pixels within a region of interest (ROI) covering the indicated neurite. Three ROIs per neurite were averaged. ROIs were selected by first determining the frame within the data series with the highest mean fluorescent intensity using Zen Blue software (Carl Zeiss Microscopy, Inc.). A rectangular ROI was then drawn on three distinct regions on three distinct neurites for a total of nine ROIs per DRG (Figure 7A). Each ROI was the same size within a DRG; to adjust the size of the set of ROIs the average fluorescence was calculated and the size (length and width) of the ROIs were adjusted until the background or non-fluorescent pixels were minimized. Fluorescent data is an average of three ROI per neurite and three neurites per DRG. Data presented as the relative change in fluorescence ($\Delta F/F_0$), where F_0 is baseline fluorescence corresponding to signal intensity before a capsaicin challenge and $\Delta F = F - F_0$ of each respective neurite as shown in Figure 7A. For all analyses the change in fluorescence was given a minimum threshold of >1% the baseline, resulting in the vehicle control group displaying a normalized value of no fluorescent change.

Next, we tested the ability to screen neuron phenotype to differentiate healthy and sensitized DRG explants in *hydrogel 1* using calcium imaging. Twenty-four-hour incubation with noxious sensitizer lipopolysaccharide (LPS, L4516, Sigma-Aldrich) lowers TRPV1+ neuron firing threshold to induce neuronal sensitization. DRGs in *hydrogel 1* were incubated with LPS at 100 ng/mL in media for 24 h. Prior to LPS incubation, DRGs were stimulated with 50 nM capsaicin (red solid) and the fluorescence was recorded with calcium imaging. Fifty nanomolars of capsaicin is below neuron firing threshold and causes no fluorescent change and therefore was used as a negative control for healthy or unsensitized neurons. After LPS incubation, DRGs were stimulated with 50 nM capsaicin and the fluorescence was recorded. Florescence was analyzed according to the methods outlined above in Section 2.4.2. A total of $n = 3$ experiments were performed with five DRGs for each experiment.

2.5 | Statistical analysis

All statistical analyses were performed using Prism 9 (GraphPad). Significant differences were determined via one-way analysis of variance (ANOVA) and Tukey's multiple comparisons tests with significance threshold $p < .05$ for diffusion, gelation, rheology, and neurite length experiments. Neurite length experiments were assessed for normality using a D'Agostino and Pearson test to determine that each experimental group (hydrogel 1 and 2 with and without MC devices) have a normal distribution of data. Analysis of florescent change for calcium imaging was performed using the Kruskal–Wallis test followed by Mann–Whitney *U* test with Bonferroni correction for each group combination to compare median fluorescent between groups at each time point. All data is displayed as $p < .05$. All data is displayed as the mean ± SD unless otherwise noted.

3 | RESULTS

3.1 | Maintaining isolation between distal neurites and DRG cell bodies

3.1.1 | Fabrication methods and design of MC device

A MC device was successfully fabricated using 3D printing with High Temp V2 resin. The culture device is cylindrical in shape; its diameter

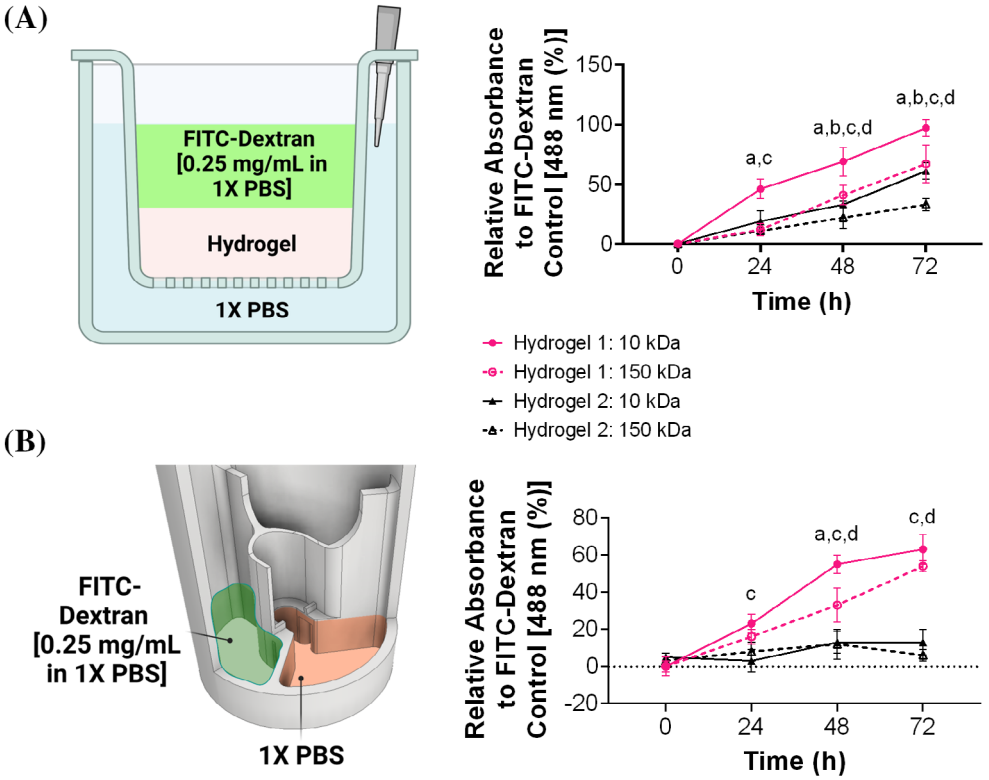

FIGURE 3 Characterizing diffusivity of hydrogel shows fluidic isolation is maintained between compartments of multicompartment (MC) device for up to 72 h. A. (Left) Schematic representing experimental setup to characterize diffusivity of hydrogels 1 and 2 using transwell insert and fluorescein isothiocyanate (FITC)-dextran solutions at 10 and 150 kDa. Hydrogel was crosslinked within transwell inserts, FITC-dextran solution (0.25 mg/mL in 1× phosphate buffered saline [PBS]) was added on top of hydrogel, and 1× PBS was added to well to match height of FITC-dextran solution to ensure diffusivity was concentration driven and not influenced by pressure gradients. Aliquots of 1× PBS were collected every 24 h up to 72 h and fluorescence was read (485 ± 45 nm excitation and 525 ± 45 nm wavelength). (Right) Absorbance of 10 and 150 kDa FITC-dextran in 1× PBS aliquots as a relative value of FITC-dextran controls from hydrogels 1 and 2. Significant differences were observed between hydrogel 1 and 2 for 10 kDa suggesting hydrogel 2 has limited diffusion compared to hydrogel 1. (B, Left) Schematic representing experimental setup to characterize diffusivity of hydrogels 1 and 2 within MC devices. Hydrogels were crosslinked in MC devices, FITC-dextran solution was added to left neurite compartment, and 1× PBS was added to the center dorsal root ganglia (DRG) compartment and right neurite compartment. Aliquots from each compartment were collected every 24 h up to 72 h and fluorescence was read (485 ± 45 nm excitation and 525 ± nm wavelength). (Right) Absorbance of 10 and 150 kDa FITC-dextran in the center compartment as a relative value of FITC-dextran controls from hydrogel 1 and 2. No significant differences were observed between the size of FITC-dextran per compartment for hydrogel 2, suggesting limited diffusion is maintained between compartments up to 22 h for particles ≤150 kDa. Only data from center compartment is displayed for ease of visualization. Schematics made in Biorender. Mean ± SD. Significant differences between groups were assessed using a one-way analysis of variance (ANOVA). $a = p < .05$ between 10 and 150 kDa for hydrogel 1. $b = p < .05$ between 10 and 150 kDa for hydrogel 2. $c = p < .05$ between 10 kDa for hydrogel 1 and 2. $d = p < .05$ between 150 kDa for hydrogel 1 and 2.

tapers from 11.61 mm at the top to 11.34 mm in diameter at its base over its height of 16.50 mm (Figure 2A). The interior of the device consists of three compartments, one DRG compartment and two neurite compartments (Figure 2B). The DRG compartment is in the center of the device and is flanked by each of the neurite compartments. Within the DRG compartment, the embedding area is 1.3 mm in width. On each side of the embedding area, a tunnel connects each of the neurite compartments to the embedding area of the DRG compartment, allowing for growth of neurons from the DRG compartment into the neurite compartments through a continuous hydrogel. Each tunnel was designed to be 0.225 mm in width, 1.0 mm in length, and 2.06 mm in height. Adding 52.9 µL hydrogel to each neurite compartment and 65.1 µL hydrogel to the DRG compartment yields a hydrogel height of 2.46 mm (Figure 2C). The average width of the fabricated tunnels, measure at 0.235 ± 0.036 mm (Figure 2B), were quantified using images taken with a microscope camera (MU1803-HS, AmScope) mounted to an inverted compound microscope (82026-630, VWR Vista Vision). A fully annotated engineering drawing of the MC device is displayed in Figure S1. Notably, High Temp V2 resin exhibits considerable autofluorescence in 488–647 nm wavelength when fully cured, which can impact imaging quality. However, we developed methods to diminish the autofluorescence using a dampening solution of 0.3% wt/vol Sudan Black B (S0593-5, Bio Basic) powder in 70% EtOH. Importantly, we assessed the effect of Sudan Black B on neurite growth using a previous device design iteration and did not observe neurite growth through both tunnels. It is possible that Sudan Black B can impact the

ability for neurites to grow through tunnels; however, the concentration can be adjusted. We chose to not use Sudan Black B in our study because we conducted immunohistochemistry after fixing cells and removed the MC devices before imaging. To use Sudan Black B, submerge MC devices in a solution of Sudan Black B (0.3% wt/vol) dissolved in 70% EtOH within 15 mL conical tubes before thermal curing. Sonicate for 30 min, remove from solution, and thermally cure as previously mentioned in Section 2.2.1. The images of resin autofluorescence before and after Sudan Black B are shown in Figure S2.

3.2 | Three-dimensional environment

3.2.1 | Characterization of hydrogel diffusivity

Diffusivity of *hydrogel 1* and *2* was assessed using a transwell insert and FITC-dextran solutions of size 10 and 150 kDa (Figure 3A). The diffusion of FITC-dextran through both hydrogel formulations showed that the lower molecular weight FITC (10 kDa) diffused 95 ± 4.6% through *hydrogel 1* and 76 ± 4.3% through *hydrogel 2* at 72 h. Higher molecular weight FITC (150 kDa) diffused 32 ± 4.8% through the *hydrogel 1* and 25 ± 4.8% through the *hydrogel 2* at 72 h (Figure 3A). These data show that particles ≤10 kDa can diffuse through both *hydrogel 1* and *2* by 72 h. However, for *hydrogel 1* and *2* the 150 kDa FITC solution did not show a significant increase between 48 and 72 h, suggesting that rate of diffusion for particles of this size is longer than a 72-h period. Together, these data show that particles ≤150 kDa can diffuse through *hydrogel 1* and *2* by 72 h. However, *hydrogel 1* has a significantly higher diffusivity than *hydrogel 2* (Figure 3A).

3.2.2 | MC Devices maintain temporal fluidic isolation between compartments

Diffusion across the MC devices was assessed by adding FITC-dextran (10 or 150 kDa) to the left neurite compartment, and 1× PBS to the center compartment and right neurite compartment on top of the hydrogel (Figure 3B). To assess diffusion across the

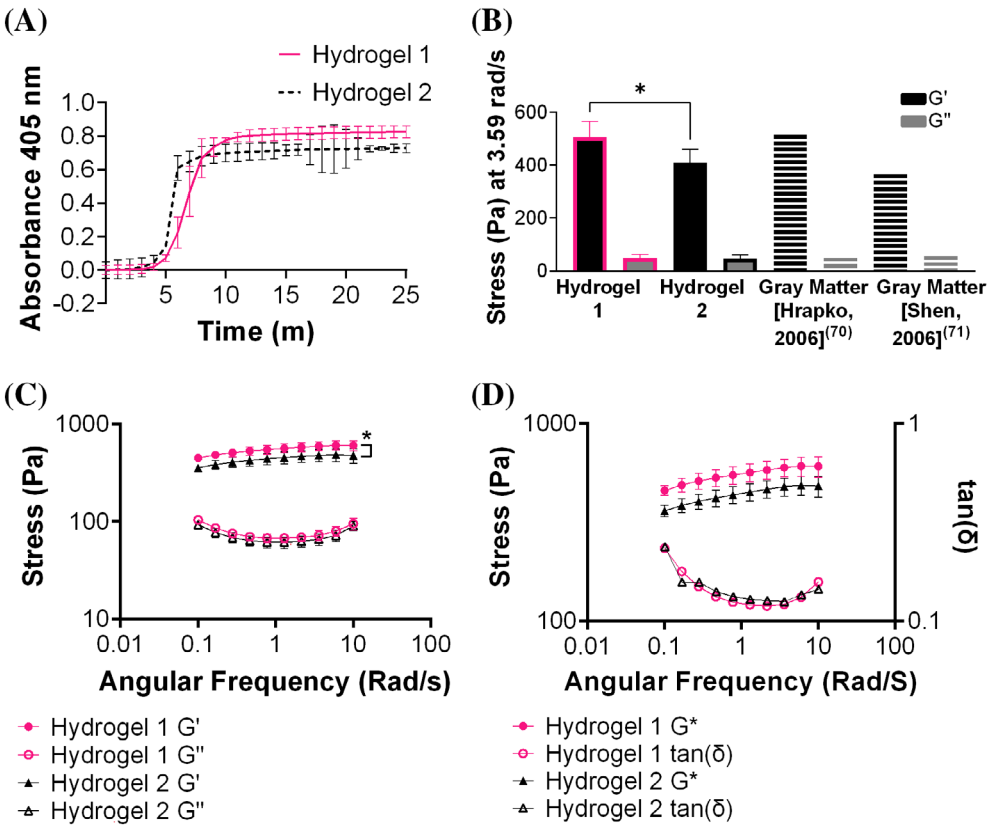

FIGURE 4 Gelation and rheological properties of hydrogels 1 and 2. (A) Change in absorbance of hydrogels 1 and 2 at 405 nm measured over time at 37°C shows collagen fibrillation occurs around 12 min for both formulations. (B) Storage (G') and loss (G'') moduli of the hydrogel formulations at 3.59 rad/s. Comparing G' and G'' of hydrogel 1 and 2 to previously published data characterizing gray matter[80,81] suggests both hydrogel formulations mimic mechanical properties of native neuronal tissue. (C) Rheological characterization of the storage (G') and loss (G'') moduli of the hydrogel formulations at an oscillatory shear strain rate of 0.1–10 rad/s. Both hydrogel formulations maintain elastic properties up to 10 rad/s. Hydrogel 1 G' is significantly greater than hydrogel 2 G'. (D) Rheological characterization of the dynamic shear modulus and tan (δ) of the hydrogel formulations shows no significant differences between hydrogel 1 and 2. Mean ± SD. Significant differences between groups were assessed using a one-way analysis of variance (ANOVA). *$p < .05$.

tunnel, the fluorescence of an aliquot from the center compartment was measured. Fluorescence of the center compartment for 10 kDa FITC for *hydrogel 1* and *2* was 63 ± 8% and 13 ± 7%, respectively at 72 h. Fluorescence of the center compartment for 150 kDa FITC for *hydrogel 1* and *2* was 54 ± 3% and 6 ± 3%, respectively (Figure 3B) at 72 h. Interestingly, for *hydrogel 1* and *2* the fluorescence did not show a significant difference between either FITC concentration from 48 to 72 h, suggesting that the 10 and 150 kDa FITC solutions reached an equilibrium point. These data show only *hydrogel 2* was able to maintain fluidic isolation between device compartments for up to 72 h for particles ≤150 kDa. Therefore, this formulation can achieve treatment isolation between the DRG cell bodies and neurites.

3.2.3 | Characterization of three-dimensional environment

For *hydrogels 1* and *2*, collagen fibrillation started at 3 min and reached 95% of the maximum absorbance by 13 min (Figure 4A) and no significant differences were observed between formulations. The storage and loss moduli of *hydrogel 1* at 3.59 rad/s were 549 ± 49 Pa and 68 ± 4 Pa, respectively. The storage modulus and loss moduli of *hydrogel 2* at 3.59 rad/s were 477 ± 35 Pa and 57 ± 6 Pa (Figure 4B,C), respectively. The storage modulus of *hydrogel 1* was significantly higher than *hydrogel 2*; however, both *hydrogel 1* and *2* maintained integrity and were robust when handled. *Hydrogel 1* maintained viscoelastic

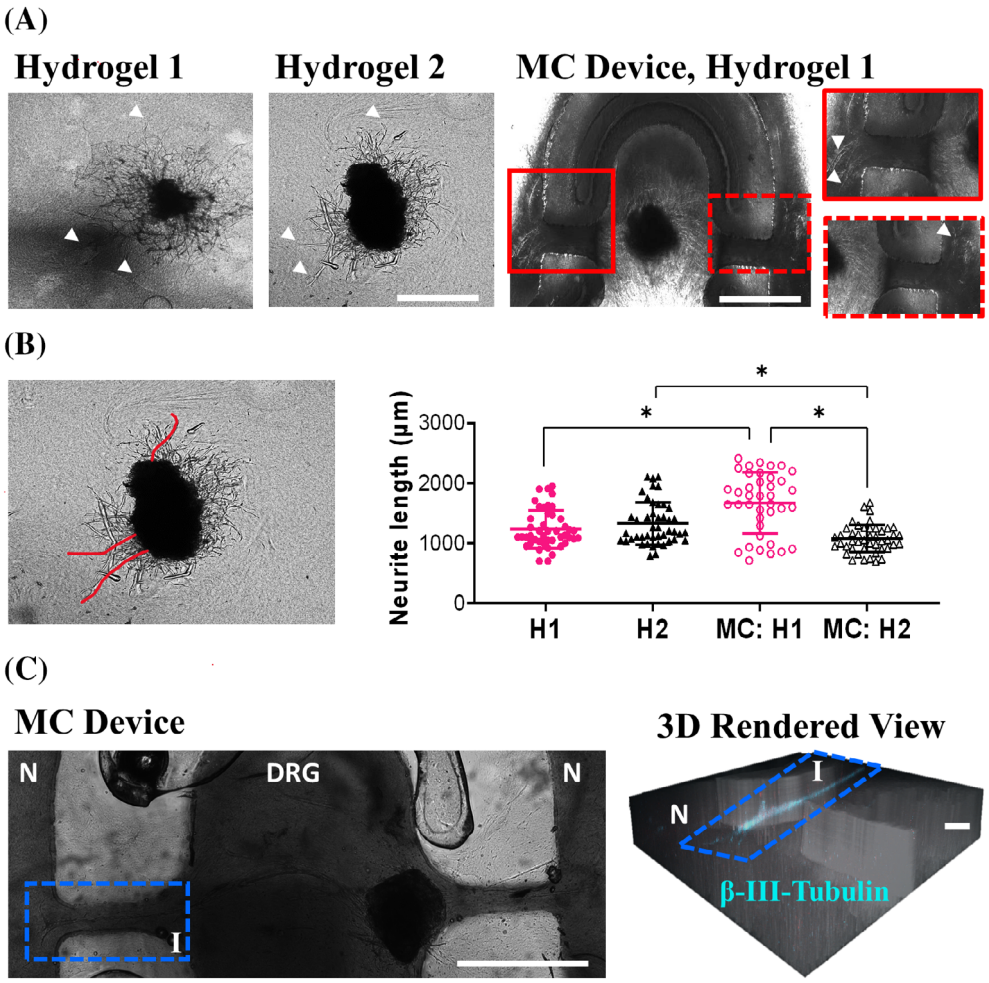

FIGURE 5 Neurite outgrowth into hydrogel 1 and 2 is maintained with multicompartment (MC) device. (A) Representative images showing neurite growth in hydrogel 1 (H1) and hydrogel 2 (H2) with and without the MC device in brightfield. Images taken with Cytation 1 (BioTek) microscope at 4× magnification. The three longest individual neurites are indicated with white arrows. Scale bar = 1000 µm. (B, Left) Representative image showing neurite tracing of the three longest neurites (red line) for quantification. (Right) Scatter plot of individual neurite lengths with average and SD of group overlayed. Three independent experiments with unique culture were performed with 3-5 dorsal root ganglia (DRGs) for each experiment. Analysis of maximum neurite length of the three longest neurites per DRG shows no significant differences between H1 and H2 suggesting both formulations promote viable neurite outgrowth. (C) Representative image of neurite outgrowth from DRG compartment into outer neurite compartments in brightfield within H1. Magnified 3D rendered image of neurite growth through the hydrogel tunnel into the outer neurite compartment (region I) stained for microtubules (cyan, β-III-Tubulin). Scale bar = 2000 µm, magnified scale bar = 10 µm. Significant differences between groups were assessed using a one-way analysis of variance (ANOVA). *$p < .05$. N, neurite compartment.

properties indicated by the dynamic shear modulus of 549 ± 51.9 Pa and tan δ of 0.157 ± 0.036 from 0.1 to 10 rad/s; *hydrogel 2* had significantly lower viscoelastic properties than *hydrogel* 1 indicated by the dynamic shear modulus of 436 ± 43.6 Pa and tan δ of 0.162 ± 0.039 from 0.1 to 10 rad/s (Figure 4D). To compare, the average storage and loss moduli from published values of white and gray matter neuronal tissue[23,78] were 510 and 43 Pa, respectively (Figure 4B) suggesting *hydrogels 1* and *2* are comparable to native neuronal tissue.

3.2.4 | Validation of DRG growth in three-dimensional MC environment

No significant differences were observed in neurite length between the control *hydrogels 1* and *2*. Maximum neurite length of the three longest neurites per DRG was 1239 ± 291 μm for control *hydrogel 1* and 1318 ± 323 μm for control *hydrogel 2* (Figure 5B). Importantly, a previous study culturing mouse DRG explants in a 3D Matrigel[85] showed robust neurite outgrowth comparable to this culture platform, suggesting this platform parallels previous literature. In addition, the maximum neurite length for DRGs embedded in MC devices within *hydrogel 2* was 1062 ± 185 μm, suggesting the presence of the MC device did not inhibit neurite growth (Figure 5B). However, we observed a significant increase in neurite length for DRGs in MC devices with *hydrogel 1* compared to MC devices with *hydrogel 2*. In addition, we observed a significant increase in neurite length for DRGs in MC devices with *hydrogel 1* compared to control *hydrogel 1*. Although significant differences were noted in neurite growth between *hydrogel 1* and *2* with MC devices, robust neurite growth in *hydrogel 2* was observed through both tunnels, suggesting both formulations are sufficient for proposed phenotypic studies. Of importance, we observed a similar yield of DRG growth with and without devices in *hydrogel 1* and *2*, where about 75% of DRGs sprouted neurites. However, we observed that about 25% of DRGs that sprouted neurites in MC devices with *hydrogels 1* and 2 grew through both tunnels. MC device culture was deemed successful when robust neurite outgrowth was observed in the outer compartments. The goal of this platform is to have significant neurite extension in the outer compartments for isolated treatment and analysis of the isolated neurites. Therefore, the 3–5 neurites that grew through both tunnels was deemed sufficient for robust experimental testing. Additional culture time or adjustments to the hydrogel formulation could be used to increase the number of neurites present in the outer compartments. Representative 2D brightfield image of neurite growth through both tunnels of the MC device stained with β-III-tubulin to show microtubules (Figure 5C, top). A magnified 3D-rendered representative image shows neurite growth through one tunnel of the hydrogel into the outer compartment, which is stained for microtubules (cyan, β-III-Tubulin) (Figure 5C, bottom). In addition, no morphological differences, including Schwann cell population, were observed for the DRGs cultured in either *hydrogel 1* or *2*. Importantly, β-III-tubulin staining of DRG neurites coincides with brightfield tracks in both plain control hydrogels and MC device (Figure S3). Together, these data show that hydrogel formulation has no effect on the ability of neurites to grow through the tunnels into the outer compartments of MC devices.

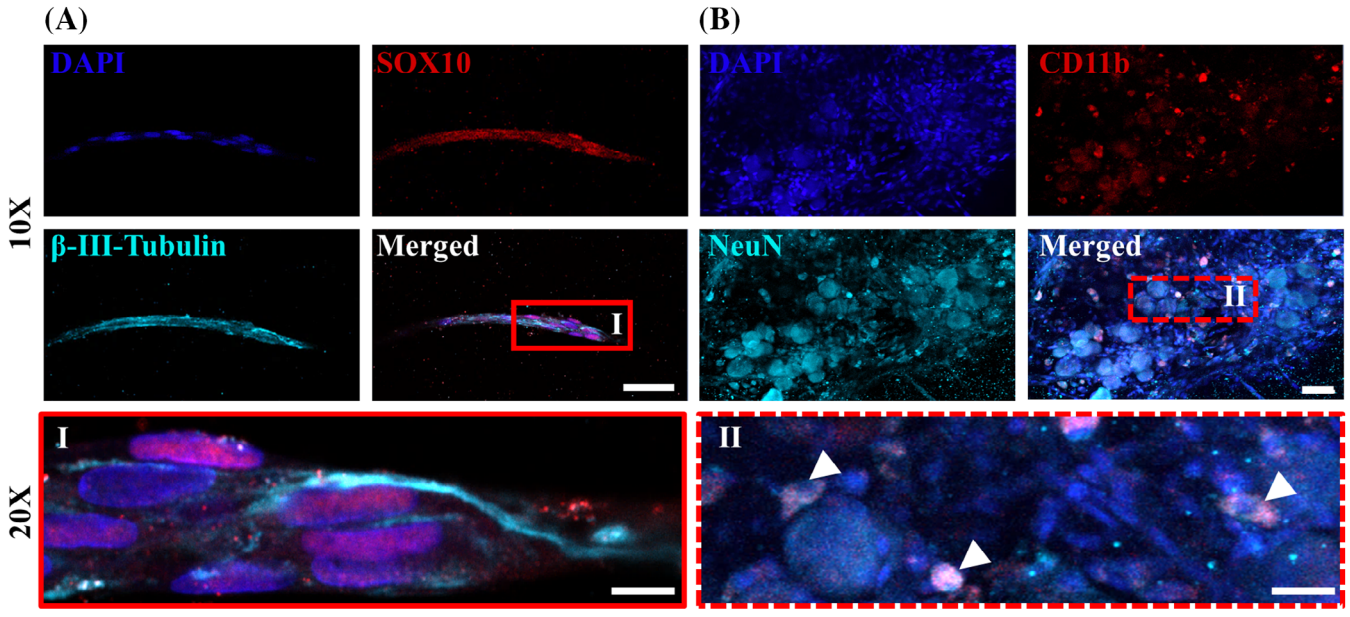

FIGURE 6 Native support cells of dorsal root ganglia (DRGs) are maintained in culture in hydrogel 1. (A) Representative individual channel images for cell nuclei (blue, DAPI). Schwann cells (red, SOX10), microtubules (cyan, β-III-Tubulin) and merged for primary sensory neurite. Magnified view of end of neurite (region I, red solid line). Scale bar = 50 μm, magnified scale bar = 10 μm. (B) Representative individual channel images for cell nuclei (blue, DAPI), macrophage/microglia marker (red, CD11b), neuronal cell bodies (cyan, NeuN) and merged for DRG explant. Magnified view of neuronal cell bodies (region II, red dashed line) show co-localization of macrophage/microglial marker and NeuN indicated by white arrows. Scale bar = 50 μm, magnified scale bar = 10 μm. Images taken with Confocal microscope (LSM 800, Carl Zeiss) at 10× or 20× magnification as indicated.

3.3 | Presence of native non-neuronal support cells

3.3.1 | Validation of native non-neuronal support cells

Immunohistochemistry revealed presence of non-neuronal support cells from explant DRGs cultured in *hydrogel 1*. Staining with SOX10 shows robust Schwann cell presence co-localized with cell nuclei (DAPI) along the extending neurite axon suggesting maintenance of Schwann cells in our culture platform (Figure 6A). Staining with NeuN for neuronal cell bodies, and CD11b for SGCs shows co-localization (white arrows) of SGCs and DAPI surrounding the neuronal cell bodies (Figure 6B). Magnified views of the distal neurite and cell bodies are displayed in Figure 6A,B.

3.3.2 | Calcium imaging displays a dose-dependent response to characterize neuronal excitability

Oregon Green BAPTA 488 (OG488, O6807, Fisher) was successfully loaded into the DRG neurons and visualized using confocal microscopy (Figure 7A). DRGs show an increase in intracellular calcium as evidenced by a fluorescent response, after a 100 nM or 1 μM capsaicin challenge with significance between 0.1 and 1 μM concentrations (Figure 7B). The maximum change in fluorescence ($\Delta F/F_0$) was a 20-fold increase in the 1 μM capsaicin and a 5-fold increase in the 0.1 μM capsaicin, with significance between groups (Figure 7C). For neuronal sensitization, we observed a significant increase between the pre- and post- LPS groups and between post-LPS and control (Figure 7D). These data demonstrate the ability to sensitize neurons with this platform and detect changes in neuronal excitability over time.

4 | DISCUSSION

4.1 | Maintaining isolation between distal neurites and DRG cell bodies

4.1.1 | Fabrication methods and design of MC device

The use of 3D printing enabled high-throughput device fabrication, allowing for a quick turnaround from design concept to fabrication. This facilitated the testing of multiple compartment geometries before arriving at the final design (Figure 2A). Furthermore, the use of 3D printing allowed this device to be made quickly, easily, and at low cost (~$1/print), given readily available access to a printer. One advantage of the High Temp V2 resin is the ability to clean and reuse MC devices, further limiting cost. To reuse MC devices, the hydrogel must first be removed from the tunnels and silicone groove. This can be achieved by soaking the devices in 70% EtOH with gentle agitation until all hydrogel residue is fully removed. Then, the devices can be autoclaved and reused. By designing the device to fit into the well of a 48-well plate, many replicates and conditions can be run on the same plate, increasing experimental throughput. Furthermore, the tapered embedding area in the final design allows for easy embedding and adjustment of DRGs.

It is also important to note Kreß et al. showed that mesenchymal stem cells co-cultured in well with a 3D printed piece of High Temp V2 resin displayed a significant decrease in cell viability and health.[86] However, since similar amounts of DRGs grew neurites in the MC devices as in plain gel controls, it indicates that our current devices are not cytotoxic. The differences in cytotoxicity of the High Temp V2 resin in this study may be explained by differences in post-processing procedures, such as an increased isopropanol wash time, the presence of heat during UV curing, and the use of a 3-h thermal cure. Each of these changes would decrease the amount of uncured resin in the 3D prints, thus reducing potential leachates. Future studies can directly probe the effect of resin cytotoxicity on cells using elution studies.

4.1.2 | MC Devices maintain temporal fluidic isolation between compartments

No differences were observed in neurite growth between *hydrogel 1* and *2* controls and the mechanical properties of both hydrogel formulations were comparable to each other (Figure 5B) and to native neuronal tissue.[80,81] However, we observed significant differences in diffusivity between *hydrogels 1* and *2*, where *hydrogel 1* had a significantly greater diffusivity than *hydrogel 2* in both transwell and MC device experiments. Therefore, to maintain spatial isolation between DRG cell bodies and sensory neurons for up to 72 h it is suggested to use *hydrogel 2*. One limitation of this system is the potential fluidic mixing between compartments after 72 h, thereby compromising the isolation between neurites and DRG cell bodies. However, previous literature has demonstrated that increasing hyaluronic acid concentration significantly increases crosslinking density, resulting in limited macromolecular diffusivity.[79] Therefore, we believe the improved diffusivity with hydrogel 2 is due to the increased concentration of MAHA compared to hydrogel 1, and fluidic isolation can be further improved with increased hydrogel stiffness. This platform has utility to temporally treat isolated neurites and probe neuronal excitability.

4.2 | Three-dimensional environment

4.2.1 | Validation of DRG growth in three-dimensional MC environment

We demonstrated the ability to culture neurites in a MC device with neurite growth through both tunnels in both *hydrogels 1* and *2* (Figure 5B). Morphologically, we observed no differences in neurite phenotype or Schwann cell populations between DRGs that were grown in *hydrogel 1* and *2* with and without MC devices. We did observe a significant increase in neurite growth with *hydrogel 1* with MC device compared to *hydrogel 2* with MC device; however, *hydrogel 2* promoted neurite growth through both tunnels demonstrating that

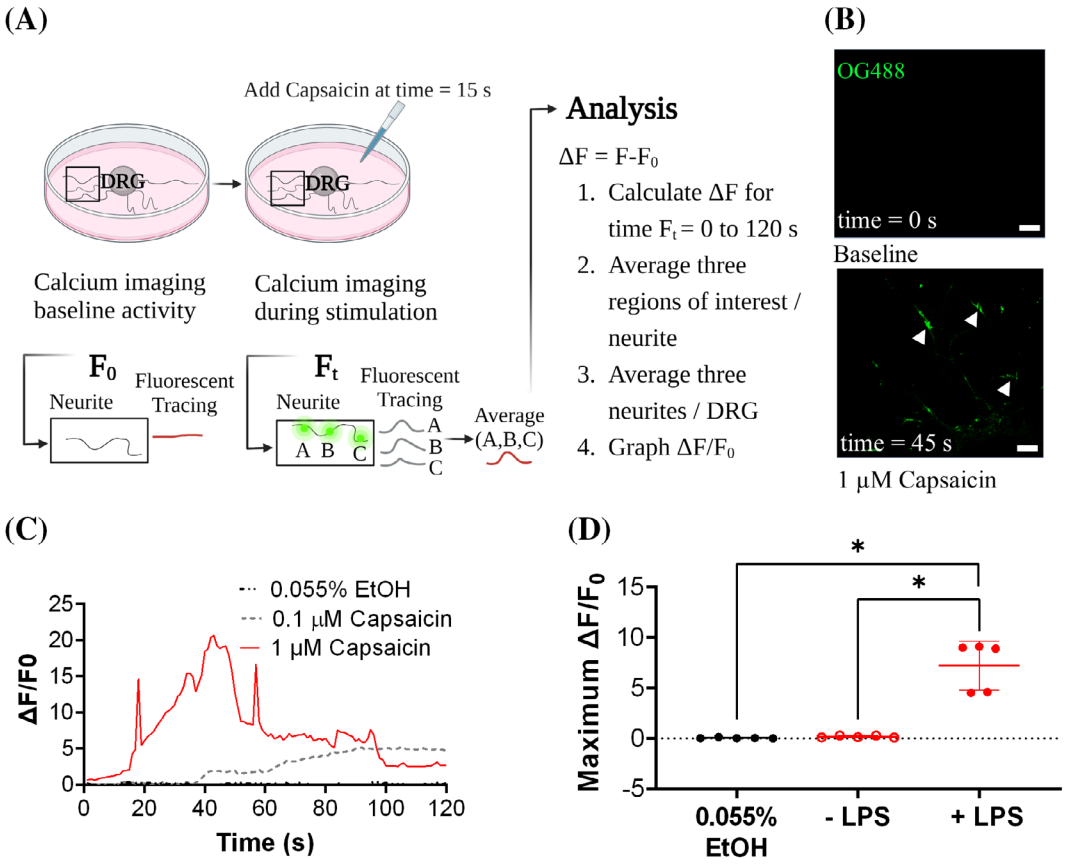

FIGURE 7 Capsaicin stimulation increases intracellular calcium concentration in neurons within dorsal root ganglia (DRG) explants embedded in hydrogel 1. (A) Schematic representing data collection and analysis for calcium imaging experiments. (B) Representative images of adult Sprague Dawley rat neurons before (top) and after (bottom) simulation with 1 µM capsaicin. White arrows show regions of increased intracellular calcium indicated by increase in fluorescence of OB488-labeled cells. Scale bar = 100 µm. (C) Tracing of fluorescent peaks plotting the relative change in fluorescence $\left(\frac{\Delta F}{F_0}\right)$ indicating an increase in calcium in response to 1 µM capsaicin (red solid), 0.1 µM capsaicin (gray dashed), and no response to 0.055% EtOH vehicle control (black hashed). Data suggests this platform can detect differences in intracellular calcium to identify neurite phenotype based on excitability. (D) 24-h lipopolysaccharide (LPS) treatment (100 ng/mL in media) resulted in the sensitization of DRGs in hydrogel 1 shown by a significant increase between the pre- and post-LPS groups and between post-LPS and control (black). Errors bars omitted from C to improve clarity. Mean ± SD. Significant differences between groups were assessed using Kruskal–Wallis and Mann–Whitney *U* tests. $^*p < .05$. Schematic made in Biorender. Oregon Green BAPTA 488, OB488.

phenotypic assays can be conducted with *hydrogel 2*. In addition, the neurite length and growth rate (data not shown) showed no significant differences when culturing DRG explants in *hydrogel 2* with or without the MC devices, suggesting presence of the MC device does not alter growth rate. One limitation of this platform is the yield of DRGs (25%) with neurite outgrowth grew through both tunnels. Future work can examine varying the MC device design or hydrogel formulation to promote guided growth through the tunnels.

4.2.2 | Characterization of three-dimensional environment

Hydrogels 1 and *2* have a stiffness comparable to that of neural tissue[80,81] making this a more translational and physiologically relevant platform to assess neuronal excitability and function than previous models (Table 1). An advantage of this system is the tunability of the hydrogel formulation, where the stiffness can be altered by adjusting the concentrations of MAHA and collagen to better mimic different target tissue stiffness, as demonstrated in the significantly different rheological properties of hydrogel 1 and 2. Our system can be modified to mimic properties of multiple tissues across the various compartments, similar to a microphysiological system (MPS). An MPS is an in vitro system to recapitulate multi-organ physiology. Several studies have used MPS to examine excitability properties of cornea neurons[87,88] suggesting ability to translate into this platform.

4.3 | Presence of native non-neuronal support cells

4.3.1 | Validation of native non-neuronal support cells

We demonstrated the presence of non-neuronal support cells in an explant DRG embedded within *hydrogel 1*, suggesting our culture

platform maintains native support cells (Figure 6A,B). This platform permits analysis of neuronal subpopulations or cell–cell interactions in one system without modification to culture conditions. Several studies have examined non-neuronal support cell and neurite interactions within various in vitro platforms; however, these studies used isolated neurons and reintroduced non-neuronal support cells following dissociation. This includes a Campenot chamber to co-culture dissociated DRGs and Schwann cells,[89] and co-culture of dissociated DRGs and glial cells in a hydrogel.[90] However, our platform is the first to promote the interactions of explanted DRGs and native non-neuronal support cells in a 3D MC device, replicating the in vivo environment. Therefore, our MC device provides a novel platform to probe the role of Schwann cells and SGCs on neurite behavior providing more physiologically relevant predictions of neuronal function and excitability. In many chronic pain states, microglia (including SGCs) can become reactive, meaning they can become activated in response to a stimulus, such as injury or inflammation. Reactive SGCs are often involved in the development and maintenance of chronic pain states. SGCs can be visualized by targeting CD11b.[91,92] Of importance, CD11b is a surface marker of macrophages and microglia, and therefore a limitation of this antibody is the potential of marking DRG macrophages in addition to SCGs.

4.3.2 | Calcium imaging displays a dose-dependent response to characterize neuronal excitability

Our platform can detect dose-dependent responses to capsaicin, thereby allowing identification of differences in neuronal excitability. It is well established that capsaicin challenges elicit a rise in intracellular calcium in neurites.[84] However, few studies have examined neuronal excitability from calcium imaging using explant DRGs,[84,93] and to our knowledge there have been no studies using explant DRGs in a hydrogel. A study by Lawrence et al.[84] used explant DRGs from mice to examine a 1 μM capsaicin challenge using fluorescent calcium imaging and reported a maximum ($\Delta F/F_0$) of 19, which compares to 23 ± 9 from our study suggesting our platform does not alter the native DRG behavior. One limitation of this study is that we did not verify the neuronal excitability of the DRGs in MC devices outside of immunofluorescent and growth analyses; however, this can be examined in future work. Based on the growth and protein characterization of the DRGs, we expect the neuronal excitability for DRGs in the MC devices to be similar to data shown above in plain gels (Figure 7C). For these studies, the calcium assay was performed in plain hydrogels without the MC device to demonstrate key phenotypic properties of DRGs. Since the neurite outgrowth was not significantly decreased between DRGs with and without the MC device and there were no morphological differences between the groups (Figure 5), it is likely that these data can be translated into the MC device. Future studies will pursue calcium imaging of DRGs in the MC device.

Despite the potential translational limitations that arise from using interspecies cells in these studies, the lack of clinical translation can largely be attributed to DRG culture conditions (such as 2D culture with dissociated neurons) that change properties of neuronal excitability.[46,74] This platform addresses these concerns by recapitulating key physiological features of DRGs including isolation between distal neurites and DRG cell bodies, a 3D environment, and presence of non-neuronal support cells thereby promoting a more translational environment.

5 | CONCLUSION

Herein we described a novel in vitro platform which mimics three essential anatomically relevant features of DRGs including fluidic isolation between DRG cell bodies and distal neurites, presence of a 3D environment, and maintenance of non-neuronal support cells. Further, we described the development of a phenotypic screening platform using calcium imaging that shows a dose-dependent response to capsaicin, demonstrating our ability to detect differences between neuronal excitability to indicate phenotype. This MC device can have a multitude of applications to both probe pathologic mechanisms in chronic pain states and screen potential therapeutics to reduce the burden of chronic pain. This platform can be used to probe changes in neuronal excitability with the goal of screening therapeutics to improve clinical translation. Lastly, the applications of this device are not limited to DRGs; various tri-culture microenvironments can be modeled and assessed in this platform, furthering insight into diseases beyond chronic pain. Future work can use different hydrogel formulations in our platform to mimic different tissues, similar to MPS. While previous culture models have shown success in the culture and evaluation of sensory neurons, there are currently no available models which utilize all three design criteria in a high-throughput screening platform adaptable for multiple cell lines, making this an attractive culture platform for probing pathologic mechanisms and screening therapeutics.

ACKNOWLEDGMENTS

Research was performed in part in the University of Nebraska-Lincoln Innovation Studio. The authors acknowledge Sarah Romereim for foundational work in the conceptualization of this in vitro device.

FUNDING INFORMATION

The research was funded in part by the NSF Career Award Grant 1846857, NSF Award 2152065 and by the NIH/NIGMS Grant T32 GM136593.

DATA AVAILABILITY STATEMENT

The data that support the findings of this study are available from the corresponding author upon reasonable request.

ORCID

Sydney M. Caparaso https://orcid.org/0000-0002-7691-9676
Adan L. Redwine https://orcid.org/0000-0002-3679-6018

REFERENCES

1. Dahlhamer J, Lucas J, Zelaya C, et al. Prevalence of chronic pain and high-impact chronic pain among adults—United States, 2016. *MMWR Morb Mortal Wkly Rep*. 2018;67:1001-1006.

2. Hardt J, Jacobsen C, Goldberg J, Nickel R, Buchwald D. Prevalence of chronic pain in a representative sample in the United States. *Pain Med*. 2008;9(7):803-812.
3. Nakamura S, Takahashi K, Takahashi Y, Yamagata M, Moriya H. The afferent pathways of discogenic low-back pain: evaluation of L2 spinal nerve infiltration. *J Bone Joint Surg Br*. 1996;78(4):606-612.
4. GBD 2017 Disease and Injury Incidence and Prevalence Collaborators. Global, regional, and national incidence, prevalence, and years lived with disability for 354 diseases and injuries for 195 countries and territories, 1990-2017: a systematic analysis for the Global Burden of Disease Study 2017. *Lancet*. 2018;392(10159):1789-1858.
5. Navratilova E, Morimura K, Xie JY, Atcherley CW, Ossipov MH, Porreca F. Positive emotions and brain reward circuits in chronic pain. *J Comp Neurol*. 2016;524(8):1646-1652.
6. Black BJ, Atmaramani R, Plagens S, et al. Emerging neurotechnology for antinoceptive mechanisms and therapeutics discovery. *Biosens Bioelectron*. 2019;126:679-689.
7. Munro G, Jansen-Olesen I, Olesen J. Animal models of pain and migraine in drug discovery. *Drug Discov Today*. 2017;22:1103-1111.
8. Mogil JS, Davis KD, Derbyshire SW. The necessity of animal models in pain research. *Pain*. 2010;151:12-17.
9. Kandasamy R, Morgan MM. 'Reinventing the wheel' to advance the development of pain therapeutics. *Behav Pharmacol*. 2021;32(2&3):142-152.
10. Burma NE, Leduc-Pessah H, Fan CY, Trang T. Animal models of chronic pain: advances and challenges for clinical translation. *J Neurosci Res*. 2017;95(6):1242-1256.
11. Moffat CJG, Vincent F, Lee JA, Eder J, Prunotto M. Opportunities and challenges in phenotypic drug discovery: an industry perspective. *Nat Rev Drug Discov*. 2017;16:531-543.
12. Basbaum AI, Bautista DM, Scherrer G, Julius D. Cellular and molecular mechanisms of pain. *Cell*. 2009;139(2):267-284.
13. Kim YS, Anderson M, Park K, et al. Coupled activation of primary sensory neurons contributes to chronic pain. *Neuron*. 2016;91(5):1085-1096.
14. Im H-J, Kim J-S, Li X, et al. Alteration of sensory neurons and spinal response to an experimental osteoarthritis pain model. *Arthritis Rheum*. 2010;62:2995-3005.
15. Ivanavicius SP, Ball AD, Heapy CG, et al. Structural pathology in a rodent model of osteoarthritis is associated with neuropathic pain: increased expression of ATF-3 and pharmacological characterisation. *Pain*. 2007;128:272-282.
16. Kanda H, Gu JG. Membrane mechanics of primary afferent neurons in the dorsal root ganglia of rats. *Biophys J*. 2017;112(8):1654-1662.
17. Kahlenberg CA, Nwachukwu BU, McLawhorn AS, Cross MB, Cornell CN, Padgett DE. Patient satisfaction after total knee replacement: a systematic review. *HSS J*. 2018;14(2):192-201.
18. malykhina a p, qin c, greenwood-van meerveld b, foreman r d, lupu f, akbarali h i. Hyperexcitability of convergent colon and bladder dorsal root ganglion neurons after colonic inflammation: mechanism for pelvic organ cross-talk. *Neurogastroenterol Motil*. 2006;18(10):936-948.
19. Kayser V, Idänpään-Heikkilä JJ, Guilbaud G. Sensitization of the nervous system, induced by two successive hindpaw inflammations, is suppressed by a local anesthetic. *Brain Res*. 1998;794:19-27.
20. Woolf CJ, Ma Q. Nociceptors—noxious stimulus detectors. *Neuron*. 2007;55(3):353-364.
21. Berta T, Qadri Y, Tan P-H, Ji R-R. Targeting dorsal root ganglia and primary sensory neurons for the treatment of chronic pain. *Expert Opin Ther Targets*. 2017;21:695-703.
22. Swinney DC, Anthony J. How were new medicines discovered? *Nat Rev Drug Discov*. 2011;10(7):507-519.
23. Jonas R, Klusch A, Schmelz M, Petersen M, Carr RW. Assessment of TTX-s and TTX-r action potential conduction along neurites of NGF and GDNF cultured porcine DRG somata. *PLoS One*. 2015;10(9):e0139107.
24. Ponce L, Heintz F, Schäfer I, et al. Isolation and cultivation of primary keratinocytes from piglet skin for compartmentalized co-culture with dorsal root ganglion neurons. *J Cell Biotechnol*. 2017;2(2):93-115.
25. Klusch A, Gorzelanny C, Reeh PW, Schmelz M, Petersen M, Sauer SK. Local NGF and GDNF levels modulate morphology and function of porcine DRG neurites, in vitro. *PLoS One*. 2018;13(9):e0203215.
26. Campenot RB, Lund K, Mok S-A. Production of compartmented cultures of rat sympathetic neurons. *Nat Protoc*. 2009;4(12):1869-1887.
27. Vogelaar CF, Gervasi NM, Gumy LF, et al. Axonal mRNAs: characterisation and role in the growth and regeneration of dorsal root ganglion axons and growth cones. *Mol Cell Neurosci*. 2009;42(2):102-115.
28. Ying Z, Misra V, Valerie MK V. Sensing nerve injury at the axonal ER: activated Luman/CREB3 serves as a novel axonally synthesized retrograde regeneration signal. *Proc Natl Acad Sci U S A*. 2014;111(45):16142-16147.
29. Ristola M, Sukki L, Azevedo MM, et al. A compartmentalized neuron-oligodendrocyte co-culture device for myelin research: design, fabrication and functionality testing. *J Micromech Microeng*. 2019;29(6):065009.
30. van de Wijdeven R, Ramstad OH, Bauer US, Halaas Ø, Sandvig A, Sandvig I. Structuring a multi-nodal neural network in vitro within a novel design microfluidic chip. *Biomed Microdevices*. 2018;20:1-8.
31. Silva DI, Santos BP d, Leng J, Oliveira H, Amédée J. Dorsal root ganglion neurons regulate the transcriptional and translational programs of osteoblast differentiation in a microfluidic platform. *Cell Death Dis*. 2017;8(12):3209.
32. Jia L, Chopp M, Wang L, Lu X, Szalad A, Zhang ZG. Exosomes derived from high-glucose–stimulated Schwann cells promote development of diabetic peripheral neuropathy. *FASEB J*. 2018;32(12):6911-6922.
33. Park JW, Vahidi B, Taylor AM, Rhee SW, Jeon NL. Microfluidic culture platform for neuroscience research. *Nat Protoc*. 2006;1(4):2128-2136.
34. Sundaramoorthy V, Green D, Locke K, O'Brien CM, Dearnley M, Bingham J. Novel role of SARM1 mediated axonal degeneration in the pathogenesis of rabies. *PLoS Pathog*. 2020;16(2):e1008343.
35. Leitão L, Neto E, Conceição F, et al. Osteoblasts are inherently programmed to repel sensory innervation. *Bone Res*. 2020;8(1):20.
36. Vysokov N, McMahon SB, Raouf R. The role of NaV channels in synaptic transmission after axotomy in a microfluidic culture platform. *Sci Rep*. 2019;9(1):1-13.
37. Jocher G, Mannschatz SH, Offterdinger M, Schweigreiter R. Microfluidics of small-population neurons allows for a precise quantification of the peripheral axonal growth state. *Front Cell Neurosci*. 2018;12:166.
38. Dumoulin A, Dagane A, Dittmar G, Rathjen FG. S-palmitoylation is required for the control of growth cone morphology of DRG neurons by CNP-induced cGMP signaling. *Front Mol Neurosci*. 2018;11:345.
39. Scholz J, Woolf C. The neuropathic pain triad: neurons, immune cells and glia. *Nat Neurosci*. 2007;10:1361-1368.
40. Schaible H-G, Richter F, Ebersberger A, et al. Joint pain. *Exp Brain Res*. 2009;196:153-162.
41. Sutton KG, Martin DJ, Pinnock RD, Lee K, Scott RH. Gabapentin inhibits high-threshold calcium channel currents in cultured rat dorsal root ganglion neurons. *Br J Pharmacol*. 2002;135:257-265. doi:10.1038/sj.bjp.0704439
42. Langford LA, Coggeshall RE. Branching of sensory axons in the peripheral nerve of the rat. *J Comp Neurol*. 1981;203(4):745-750.
43. Spray DC, Hanani M. Gap junctions, pannexins and pain. *Neurosci Lett*. 2019;695:46-52.
44. Gross PG, Kartalov EP, Scherer A, Weiner LP. Applications of microfluidics for neuronal studies. *J Neurol Sci*. 2007;252:135-143.
45. Campenot RB. Local control of neurite development by nerve growth factor. *Proc Natl Acad Sci U S A*. 1977;74:4516-4519.

46. Nascimento AI, Mar FM, Sousa MM. The intriguing nature of dorsal root ganglion neurons: linking structure with polarity and function. *Prog Neurobiol*. 2018;168:86-103.
47. Neto E, Leitao L, Sousa DM, et al. Compartmentalized microfluidic platforms: the unrivaled breakthrough of in vitro tools for neurobiological research. *J Neurosci*. 2016;36(46):11573-11584.
48. Breslin S, O'Driscoll L. Three-dimensional cell culture: the missing link in drug discovery. *Drug Discov Today*. 2013;18:240-249.
49. Duval K, Grover H, Han L-H, et al. Modeling physiological events in 2D vs. 3D cell culture. *Phys Ther*. 2017;32(4):266-277.
50. Fornaro M, Sharthiya H, Tiwari V. Adult mouse DRG explant and dissociated cell models to investigate neuroplasticity and responses to environmental insults including viral infection. *J Vis Exp*. 2018;133:56757.
51. Liu R, Lin G, Xu H. An efficient method for dorsal root ganglia neurons purification with a one-time anti-mitotic reagent treatment. *PLoS One*. 2013;8(4):e60558.
52. Song Y, Gao L. The effect of acute dissociation on the electrophysiological properties of rat dorsal root ganglion neurons. *Somatosens Mot Res*. 2018;35(1):11-17.
53. Li GN, Livi LL, Gourd CM, Deweerd ES, Hoffman-Kim D. Genomic and morphological changes of neuroblastoma cells in response to three-dimensional matrices. *Tissue Eng*. 2007;13:1035-1047.
54. Lee J, Cuddihy MJ, Kotov NA. Three-dimensional cell culture matrices: state of the art. *Tissue Eng Part B Rev*. 2008;14:61-86.
55. Desai A, Kisaalita WS, Keith C, Wu ZZ. Human neuroblastoma (SH-SY5Y) cell culture and differentiation in 3-D collagen hydrogels for cell-based biosensing. *Biosens Bioelectron*. 2006;21:1483-1492.
56. Ju YE, Janmey PA, McCormick ME, Sawyer ES, Flanagan LA. Enhanced neurite growth from mammalian neurons in three-dimensional salmon fibrin gels. *Biomaterials*. 2007;28:2097-2108.
57. Lee YS, Collins G, Arinzeh TL. Neurite extension of primary neurons on electrospun piezoelectric scaffolds. *Acta Biomater*. 2011;7:3877-3886.
58. Jensen C, Yong T. Is it time to start transitioning from 2D to 3D cell culture. *Front Mol Biosci*. 2020;7:1-15.
59. Ren Y, Suter DM. Increase in growth cone size correlates with decrease in neurite growth rate. *Neural Plast*. 2016;2016:3497901.
60. Seidlits SK, Khaing ZZ, Petersen RR, et al. The effects of hyaluronic acid hydrogels with tunable mechanical properties on neural progenitor cell differentiation. *Biomaterials*. 2010;31(14):3930-3940.
61. Lin PW, Wu CC, Chen CH, Ho HO, Chen YC, Sheu MT. Characterization of cortical neuron outgrowth in two- and three-dimensional culture systems. *J Biomed Mater Res B Appl Biomater*. 2005;75:146-157.
62. Esper RM, Loeb JA. Rapid axoglial signaling mediated by neuregulin and neurotrophic factors. *J Neurosci*. 2004;24:6218-6227.
63. Austin PJ, Moalem-Taylor G. The neuro-immune balance in neuropathic pain: involvement of inflammatory immune cells, immune-like glial cells and cytokines. *J Neuroimmunol*. 2010;229:26-50.
64. Campana WM. Schwann cells: activated peripheral glia and their role in neuropathic pain. *Brain Behav Immun*. 2007;21:522-527. doi:10.1016/j.bbi.2006.12.008
65. Hanani M. Satellite glial cells in sensory ganglia: from form to function. *Brain Res Brain Res Rev*. 2005;48:457-476.
66. Watkins LR, Maier SF. Beyond neurons: evidence that immune and glial cells contribute to pathological pain states. *Physiol Rev*. 2002;82:981-1011.
67. Ahmed I, Ponery AS, Nur EKA, et al. Morphology, cytoskeletal organization, and myosin dynamics of mouse embryonic fibroblasts cultured on nanofibrillar surfaces. *Mol Cell Biochem*. 2007;301:241-249.
68. Chang SS, Guo WH, Kim Y, Wang YL. Guidance of cell migration by substrate dimension. *Biophys J*. 2013;104:313-321.
69. Weaver VM, Petersen OW, Wang F, et al. Reversion of the malignant phenotype of human breast cells in three-dimensional culture and in vivo by integrin blocking antibodies. *J Cell Biol*. 1997;137:231-245.
70. Hyland C, Mertz AF, Forscher P, Dufresne E. Dynamic peripheral traction forces balance stable neurite tension in regenerating Aplysia bag cell neurons. *Sci Rep*. 2014;4:4961.
71. Carozzi VA, Salio C, Rodriguez-Menendez V, Ciglieri E, Ferrini F. 2D *vs* 3D morphological analysis of dorsal root ganglia in health and painful neuropathy. *Eur J Histochem*. 2021 Oct 19;65(s1):3276. doi:10.4081/ejh.2021.3276
72. Lai Y, Cheng K, Kisaalita W. Three dimensional neuronal cell cultures more accurately model voltage gated calcium channel functionality in freshly dissected nerve tissue. *PLoS One*. 2012;7:e45074.
73. Phillips MJ, Otteson DC. Differential expression of neuronal genes in Muller glia in two- and three-dimensional cultures. *Invest Ophthalmol Vis Sci*. 2011;52:1439-1449.
74. Park JW, Kim HJ, Kang MW, Jeon NL. Advances in microfluidics-based experimental methods for neuroscience research. *Lab Chip*. 2013;13:509-521.
75. Wachs RA, Hoogenboezem EN, Huda HI, Xin S, Porvasnik SL, Schmidt CE. Creation of an injectable in situ gelling native extracellular matrix for nucleus pulposus tissue engineering. *Spine J*. 2017;17(3):435-444.
76. Romereim SM, Johnston CA, Redwine AL, Wachs RA. Development of an in vitro intervertebral disc innervation model to screen neuroinhibitory biomaterials. *J Orthop Res*. 2020;38(5):1016-1026.
77. Suri S, Schmidt CE. Cell-laden hydrogel constructs of hyaluronic acid, collagen, and laminin for neural tissue engineering. *Tissue Eng Part A*. 2010;16(5):1703-1716.
78. Piening LM, Lillyman DJ, Lee FS, Lozano AM, Miles JR, Wachs RA. Injectable decellularized nucleus pulposus tissue exhibits neuroinhibitory properties. *JOR Spine*. 2022;5(1):e1187.
79. Bian L, Hou C, Tous E, Rai R, Mauck RL, Burdick JA. The influence of hyaluronic acid hydrogel crosslinking density and macromolecular diffusivity on human MSC chondrogenesis and hypertrophy. *Biomaterials*. 2013;34(2):413-421.
80. Hrapko M, van Dommelen J, Peters GW, Wismans JS. The mechanical behaviour of brain tissue: large strain response and constitutive modelling. *Biorheology*. 2006;43(5):623-636.
81. Shen F, Tay TE, Li JZ, Nigen S, Lee PV, Chan HK. Modified Bilston nonlinear viscoelastic model for finite element head injury studies. *J Biomech Eng*. 2006;128:797-801.
82. Liu Z, Jin Y-Q, Chen L, et al. Specific marker expression and cell state of Schwann cells during culture in vitro. *PLoS One*. 2015;10(4):e0123278.
83. Grienberger C, Konnerth A. Imaging calcium in neurons. *Neuron*. 2012;73(5):862-885. doi:10.1016/j.neuron.2012.02.011
84. Lawrence GW, Zurawski TH, Oliver Dolly J. Ca^{2+} signalling induced by NGF identifies a subset of capsaicin-excitable neurons displaying enhanced chemo-nociception in dorsal root ganglion explants from adult pirt-GCaMP3 mouse. *Int J Mol Sci*. 2021;22(5):2589.
85. Klimovich P, Rubina K, Sysoeva V, Semina E. Three-dimensional model of dorsal root ganglion explant as a method of studying neurotrophic factors in regenerative medicine. *Biomedicine*. 2020;8(3):49.
86. Kreß S, Schaller-Ammann R, Feiel J, Priedl J, Kasper C, Egger D. 3D printing of cell culture devices: assessment and prevention of the cytotoxicity of photopolymers for stereolithography. *Materials*. 2020;13(13):3011.
87. Deardorff PM, McKay TB, Wang S, et al. Modeling diabetic corneal neuropathy in a 3D in vitro cornea system. *Sci Rep*. 2018;8(1):17294.

88. Siran W, Ghezzi CE, Cairns DM, et al. Human corneal tissue model for nociceptive assessments. *Adv Healthc Mater*. 2018;7(19):1800488.
89. Xiao J, Wong AW, Willingham MM, et al. BDNF exerts contrasting effects on peripheral myelination of NGF-dependent and BDNF-dependent DRG neurons. *J Neurosci*. 2009;29(13):4016-4022.
90. Yamada A, Renault R, Chikina A, et al. Transient microfluidic compartmentalization using actionable microfilaments for biochemical assays, cell culture and organs-on-chip. *Lab Chip*. 2016;16(24):4691-4701.
91. Cao H, Zhang Y-Q. Spinal glial activation contributes to pathological pain states. *Neurosci Biobehav Rev*. 2008;32(5):972-983.
92. Ohara PT, Vit J-P, Bhargava A, et al. Gliopathic pain: when satellite glial cells go bad. *Neuroscientist*. 2009;15(5):450-463.
93. Miller RE, Weidler C, Falk W, et al. Damage-associated molecular patterns generated in osteoarthritis directly excite murine nociceptive neurons through Toll-like receptor 4. *Arthritis Rheumatol*. 2015;50:1156-1163.

SUPPORTING INFORMATION

Additional supporting information can be found online in the Supporting Information section at the end of this article.

How to cite this article: Caparaso SM, Redwine AL, Wachs RA. Engineering a multicompartment in vitro model for dorsal root ganglia phenotypic assessment. *J Biomed Mater Res*. 2023;1-18. doi:10.1002/jbm.b.35294